Development 138, 3247-3259 (2011) doi:10.1242/dev.063768

Muscle force regulates bone shaping for optimal load-bearing capacity during embryogenesis

Amnon Sharir[1,2], Tomer Stern[1], Chagai Rot[1], Ron Shahar[2,*] and Elazar Zelzer[1,*]

SUMMARY

The vertebrate skeleton consists of over 200 individual bones, each with its own unique shape, size and function. We study the role of intrauterine muscle-induced mechanical loads in determining the three-dimensional morphology of developing bones. Analysis of the force-generating capacity of intrauterine muscles in mice revealed that developing bones are subjected to significant and progressively increasing mechanical challenges. To evaluate the effect of intrauterine loads on bone morphogenesis and the contribution of the emerging shape to the ability of bones to withstand these loads, we monitored structural and mineral changes during development. Using daily micro-CT scans of appendicular long bones we identify a developmental program, which we term preferential bone growth, that determines the specific circumferential shape of each bone by employing asymmetric mineral deposition and transient cortical thickening. Finite element analysis demonstrates that the resulting bone structure has optimal load-bearing capacity. To test the hypothesis that muscle forces regulate preferential bone growth in utero, we examine this process in a mouse strain (mdg) that lacks muscle contractions. In the absence of mechanical loads, the stereotypical circumferential outline of each bone is lost, leading to the development of mechanically inferior bones. This study identifies muscle force regulation of preferential bone growth as the module that shapes the circumferential outline of bones and, consequently, optimizes their load-bearing capacity during development. Our findings invoke a common mechanism that permits the formation of different circumferential outlines in different bones.

KEY WORDS: Bone shape, Periosteal growth, Muscle contraction, Mechanical load, Mineralization, Micro-CT, Mouse

INTRODUCTION

Although the shape of an organ is fundamental to its functionality, relatively little is known about the mechanisms that regulate organ morphogenesis. The complexity in deciphering these mechanisms in bones is even greater, as each bone has its unique morphological features. The diversity of bone design has played a pivotal role in the evolutionary success of vertebrates. It has enabled the skeleton to provide form and stability while maintaining mobility under varying loading scenarios and under changing evolutionary pressures (Currey, 2003). Most of the bones develop by endochondral ossification, a process whereby an anlage of cartilage is gradually replaced by mineralized tissue (Streeter, 1949). Bone longitudinal growth and cartilage replacement are regulated by the growth plate, which is located near the ends of long bones and is composed of chondrocytes that undergo a well defined and highly controlled differentiation program (Karsenty and Wagner, 2002; Kronenberg, 2003; Olsen et al., 2000).

The process of endochondral ossification is an efficient way to build a new bone over a pre-existing cartilaginous template and to allow it to grow in length. However, the main feature of this process also represents its limitation, as it cannot form a shape that is missing from the template or operate in places along the shaft from which the growth plate has already retreated. Hence, the rapid growth and morphological changes that occur during bone development must be brought about by a process other than endochondral ossification.

When considering the mechanisms that underlie the developmental process that shapes bones, of special interest is the question of tissue-autonomous versus non-autonomous regulation, in other words, the possible involvement of signals from other tissues. Muscle-induced mechanical signals provide an example of such external contribution. Post-developmentally, there is a large body of evidence that supports the involvement of muscles and the mechanical load that they apply on the bone in determining its 3D morphology. Bones remodel throughout life in order to adapt to their mechanical environment (Frost, 2001). Accordingly, increased physical activity in children affects the geometry and composition of their bones, whereas decreased loads due to enforced rest or muscle dysfunctions result in thinner bones (Schoenau, 2005; Ward et al., 2006). Furthermore, it has been shown that the relationship between bone morphology and muscle force is reciprocal, as the shape of a bone determines the load that it can tolerate (Frost, 2001; Weiner and Wagner, 1998).

In contrast to this wealth of available information, much less is known about the involvement of the musculature or other surrounding tissues in the embryonic bone shaping processes. The involvement of muscles in several aspects of skeletogenesis, such as joint formation, longitudinal growth and bone ridge formation (Blitz et al., 2009; Hall, 1971; Hall and Kalliecharan, 1975; Hosseini and Hogg, 1991; Kahn et al., 2009; Nowlan et al., 2008), supports a potential contribution of muscles to the mechanism that allows different bones to acquire different shapes. However, in vitro studies of chick embryos in which bone segments were cultured using various experimental protocols found that, apart from varying delays in the mineralization process, the overall shape

[1]Department of Molecular Genetics, Weizmann Institute of Science, Rehovot 76100, Israel. [2]Koret School of Veterinary Medicine, The Robert H. Smith Faculty of Agriculture, Food and Environment, The Hebrew University of Jerusalem, Rehovot 76100, Israel.

*Authors for correspondence (shahar@agri.huji.ac.il; eli.zelzer@weizmann.ac.il)

Accepted 21 May 2011

of the bone rudiments was unaffected (Bradley, 1970; Hamburger and Waugh, 1940; Murray and Selby, 1930). Moreover, a study of the regulation of rib curvature identified differential expression of *Bmp5* around the surface of the ribs determined by anatomy-specific enhancers, supporting the autonomous nature of bone shaping (Guenther et al., 2008). Yet, it is unclear whether the mechanism that shapes the ribs is also responsible for shaping other bones. Given this conflicting evidence, the issue of bone shaping regulation remains to be resolved.

In this work, we identify a novel developmental program that shapes long bones, regulating their circumferential outline through asymmetric mineral deposition and transient cortical thickening. We show that this program enables developing bones to withstand rapidly increasing mechanical loads applied to them by the musculature. At the same time, this unique program is regulated by intrauterine muscle contractions, as in their absence the typical shape and mechanical integrity of bones are lost.

MATERIALS AND METHODS

Animals

C57BL/6 mice were purchased from Harlan Laboratories (Jerusalem, Israel). For the developmental analysis, only C57BL/6 males were analyzed. Embryo sex was determined by PCR (McClive and Sinclair, 2001); after birth, it was determined by external examination. At every developmental stage excluding P6, six to eight mice from at least three different litters were evaluated. At P6, two to four mice from two different litters were examined.

Mice heterozygous for the mutation muscular dysgenesis (mdg) (Pai, 1965a; Pai, 1965b) were kindly provided by G. Kern (Innsbruck Medical University, Innsbruck, Austria). *Runx2* heterozygous mice (Komori et al., 1997), used for detection of osteoblasts, and *Pax3-Cre* (Engleka et al., 2005) and ROSA-YFP reporter mice (Srinivas et al., 2001), used for visualization and isolation of muscles, were purchased from Jackson Laboratory (Bar Harbor, ME, USA). To overexpress *Vegf* in osteoblasts, *Col1a1-Cre* (Dacquin et al., 2002), *tet-Vegf*$_{164}$ (Dor et al., 2002) and ROSA26-rtTA (Belteki et al., 2005) mouse lines were crossed to generate triple-transgenic mice. *Vegf* expression was induced by adding 200 μg/ml doxycycline hydrochloride (Sigma, D9891) in 3% sucrose to the drinking water of pregnant females from E13.5 until birth. As a control, age-matched double-transgenic littermates were used. The effect of osteoclastic activity was examined in a mouse strain that carries a null mutation in the Rous sarcoma oncogene (*Src*) gene. In this mutant, a deficiency of osteoclast function occurs, leading to osteopetrosis (Soriano et al., 1991). *Src* mice were purchased from Jackson Laboratory.

In all timed pregnancies, plug date was defined as E0.5. For harvesting of embryos, timed-pregnant females were sacrificed by CO_2 intoxication. The gravid uterus was dissected out and suspended in a bath of cold phosphate-buffered saline (PBS), and the embryos were harvested after amnionectomy and removal of the placenta. Tail genomic DNA was used for genotyping.

Micro-computed tomography (micro-CT) analysis

Samples were micro-CT scanned (eXplore Locus SP, GE Healthcare, London, Ontario, Canada) at 45 kV and 120 μA. For all scans, 900 projections at a total integration time of 2850 mseconds resulted in a nominal isotropic resolution of 7 μm. Calibration hydroxyapatite phantoms (GE Medical) were used to facilitate conversion of the linear attenuation of a given voxel to mg HA/cm^3. Three-dimensional patterns of bone morphology and mineralization were visualized and quantified using a novel approach that we term 'computational skeletography' (to be reported elsewhere).

Preprocessing stages included multiple image registration for each subset of bones of the same type to ensure positional correspondence (rigid registration, six degrees of freedom), image segmentation, i.e. separation of bone from background voxels by automatic global threshold, and manual isolation of volume of interest (VOI) to serve as the anatomic domain of all downstream analyses, with the exception of cluster analysis (see below).

The VOI was defined in the mid-diaphysis because (1) changes were expected to be most noticeable at this location, at which periosteal bone growth commences, and (2) this region was assumed to experience the greatest bending stresses (Rubin and Lanyon, 1984). Each VOI consists of a series of consecutive transverse slices covering 4% of the bone length. Variables were evaluated for each slice separately and then averaged for the entire VOI. Variables were measured either for the entire cortical cross-section or as vector variables. Overall values were calculated according to standard formulas (not shown), averaged over each subset of VOIs, defined as bones of the same type and developmental stage, and standard deviation was calculated. Vector variables relate to a polar coordinate system superimposed on the transverse image. The pole was defined as the geometric center of the putative region of the cartilaginous anlage and the polar axis was defined as the craniocaudal axis, with zero degrees at the caudal aspect.

To conduct these analyses we used a newly developed method for analysis and visualization of long bone mineralization and morphology, which we term 'unroll transformation' (see Fig. S5 in the supplementary material; to be described in detail elsewhere). Following transformation, each variable was calculated separately for each angular coordinate. Finally, all vectors of the same variable were averaged over each subset of VOIs. Several properties, such as cortical thickness and tissue mineral density (TMD), were determined both for the entire cortex and for each angular coordinate.

Skeletal preparations

Cartilage and bone in whole mouse embryos were visualized after staining with Alcian Blue and Alizarin Red S (Sigma) and clarification of soft tissue with KOH (McLeod, 1980).

Histology and in situ hybridization

Limbs were fixed overnight in 4% paraformaldehyde (PFA) in PBS and decalcified at 4°C in 19% EDTA (pH 7.4) for 1-12 days, depending on the developmental stage. Then, tissues were dehydrated to 100% ethanol, embedded in paraffin and sectioned at 5 μm. Osteoclasts were detected using a TRAP staining kit (Sigma). Section in situ hybridizations were performed as described previously (Murtaugh, 1999; Riddle et al., 1993).

Evaluation of bone deposition and resorption

Bone deposition and resorption were evaluated by intraperitoneal injections of Calcein (Sigma, C0875; 2.5 mg/kg body weight) into pregnant females at E15 and Alizarin Complexone (Sigma, a3882; 7.5 mg/kg) at E16 or Calcein Blue (Sigma, M1255; 7.5 mg/kg) at E17. The harvested limbs were fixed overnight in 4% PFA in PBS, following which tissues were dehydrated to 100% ethanol, embedded in paraffin and sectioned at 7 μm. Fluorescence was visualized by confocal microscopy (Leica DMI 4000B).

Whole-mount β-galactosidase staining

Embryos were fixed for 1 hour in 4% PFA at 4°C, washed three times in rinse buffer (0.01% deoxycholate, 0.02% NP40, 2 mM $MgCl_2$, 5 mM EGTA in PBS) at room temperature and then stained for 3 hours at 37°C in rinse buffer supplemented with 1 mg/ml X-Gal, 5 mM $K_3[Fe(CN)_6]$ and 5 mM $K_4[Fe(CN)_6]$. For histological examination, stained whole-mount limbs were fixed in 4% PFA overnight, dehydrated and embedded in paraffin. Then, 5 μm sections were collected and mounted on Fisherbrand Superfrost Plus slides, dehydrated and cleared in xylene.

Muscle functional assessment

The triceps brachii, tibialis anterior and biceps femoris muscles of *Pax3-Cre*/ROSA-YFP mice were individually identified, isolated and removed under a binocular fluorescence microscope and then weighed on an analytical scale. Measurement precision was ±0.01 mg. Muscle masses were evaluated in ten mice from three different litters. Average weights and standard deviations were calculated for each muscle.

Mechanical testing

Mechanical testing of samples was carried out on eight radii from each of the following age groups: E17.5, P1 and P6. Bones were tested by three-point bending (Robling and Turner, 2002) using a custom-made miniature testing

machine, which has a force resolution of 0.015 N (AL311BN-6I, Sensotec, Honeywell, USA). Radii were chosen owing to their relatively long, straight and close-to cylindrical morphology and their high aspect ratio (Schriefer et al., 2005). Radii were removed under microscopic control immediately before testing under microscopic control, cleaned of adhering soft tissue and placed on two supports with rounded profiles (0.2 mm diameter), such that the supports were located equidistant from the ends of the bone and at the maximum feasible distance from each other. The support distances were as follows: 1.3 mm for E17.5, 1.5 mm for P1 and 2.6 mm for P6. Each bone was loaded on its posterior aspect at the point corresponding to the mid-distance between the bottom supports. Radii were fixed in place using a 0.01 N static preload and then immersed in saline. Ten preload cycles (0 to 0.01 N) were applied in order to allow the bone to accommodate to the load. Monotonic loading was then conducted at a constant rate (0.1 mm/minute) up to fracture or to a maximum displacement of 300 μm. Force-displacement data were collected at 20 Hz. The resulting load-displacement curves were used to calculate stiffness (Turner and Burr, 1993), defined as the slope of the linear portion of the load-displacement curve. Young's modulus was approximated by using beam theory and $E=S\cdot L^3/48\cdot I$, where E is the effective Young's modulus (N/mm^2), S is the slope of the linear portion of the load-displacement curve (N/mm), L is the support span (mm) and I is the cross-sectional moment of inertia (mm^4) determined at the area of fracture by micro-CT.

Finite element models

Reconstructed micro-CT scans of femora from wild-type mice at E18 and P6 and from E18 mdg mutants, consisting of 285 (E18.5) and 584 (P6) 2D images of transverse slices, were imported into an image manipulation software package (Amira 4.1.2, Visage Imaging, Carlsbad, CA, USA). Images were segmented by selecting an appropriate threshold and used to create 3D geometry. The resulting 3D object was meshed with four-node tetrahedral elements, thus yielding a 3D finite element model of each bone. The meshed model was then exported into a finite element analysis software package (Patran 2008r1, MSC Software Corporation, Santa Ana, CA, USA).

In order to quantify the contribution of asymmetric distribution of mass and of curvature to bending resistance of long bones, two additional, idealized models were created based on the P6 bone model. Periosteal and endosteal perimeters and the position of the centroid of seven equally spaced segments along the long axis of the bone were obtained from the scans. These data were used first to create a model of a straight tube, equal in length to the P6 femur. At each of these seven cross-sections, the inner circle was made equal in area to the endosteal area of the P6 femur and the outer circle equal in area to the area inside the periosteum; the rest of the tube was created by extrapolation between these cross-sections. The resulting model was a straight tube, with its mass, which was similar to that of the actual bone, symmetrically distributed, unlike in the actual bone. The second idealized bone model was created similarly; however, the centers of its seven tubular cross-sections were made to coincide with the positions of the respective centroids of the actual bone, thus resulting in a tube similar to the previous one, but with a curvature similar to that of the actual bone. Bone material was assumed homogeneous, isotropic and linearly elastic. Material properties were assigned as follows: Young's modulus, as determined experimentally in this study (0.2 GPa for E18.5 and 0.8 GPa for P6) and Poisson's ratio, based on values reported in the literature (0.2) (Shahar et al., 2007). Several nodes at the distal end of the model were fully restrained to anchor the model. All models were subject to two loading scenarios: a bending force was applied at a proximal location and directed either medially (see Fig. 4A, purple arrow), which is a physiological muscle force orientation, or cranially (see Fig. 4A, blue arrow). Finite element analysis of these models yielded displacement, stress and strain distributions through the entire bone. Strain distribution in the z (axial) direction is shown because this is the most relevant in a beam-bending scenario.

Statistical methods

All variables measured in this study were quantitative. Variables are presented as mean ± s.d. In each of the measured variables, change as a function of age was assessed by the non-parametric Kruskal-Wallis test. The comparison between two consecutive time points was carried out using the Mann-Whitney non-parametric test, applying Holm-Bonferroni correction of the significance level for multiple pairwise comparisons. The Mann-Whitney test was also used for comparison of control with mdg genotype, per bone type and per age. All tests were two-tailed and statistical significance was defined as a $P\leq 0.05$.

RESULTS

Developing bones are exposed to increasing mechanical stresses

The magnitude of mechanical loads applied to bones by the musculature during development is unknown. In order to evaluate the possible role of the musculature in the shaping of developing bones and in their resulting mechanical properties, it is necessary to assess the mechanical challenges that these bones face. To this end, we first measured the increase in muscle force-generating capacity and in lever arm, which have been shown to significantly increase the magnitude of bending loads acting upon bones (Fig. 1A) (Brear et al., 1990; Currey, 1999). Between E17.5 and P6, long bones increased in length ~3-fold (Fig. 1B) and muscles attached to them increased their mass and consequently their force-generating potential (Gokhin et al., 2008) ~5-fold (Fig. 1C). Therefore, when making comparisons among muscles that contract to their maximum capacity, the combined outcome of these two processes is an up to 15-fold increase in the potential bending moment, and hence in the potential stresses encountered by these bones.

To demonstrate in vivo the effect of intrauterine mechanical loads on the developing skeleton, we interfered with the normal process of bone formation and examined the effect on bone integrity. It has been shown previously that vascular endothelial growth factor (*Vegf*) overexpression during bone development leads to an increase in blood vessel formation, followed by abnormal mineral deposition (Maes et al., 2010). Scanned E18.5 embryos in which *Vegf* was overexpressed (*Vegf*-OE) in osteoblasts clearly demonstrated that, although total mineral content was comparable to that of control skeletons (see Fig. S1 in the supplementary material), the mutants exhibited abnormal cortex formation and mid-diaphyseal fractures in all the long bones (Fig. 1D).

To substantiate the causal relationship between intrauterine muscle forces and the mid-diaphyseal fractures that we observed in *Vegf*-OE bones, we examined bone development in embryos that overexpress *Vegf* but lack muscle contractility. We crossed *Vegf*-OE mice with the muscular dysgenesis (mdg) mouse strain, which carries a naturally occurring autosomal recessive mutation (in *Cacna1s* – Mouse Genome Informatics). This mouse lacks excitation-contraction coupling, leading to the absence of skeletal muscle contractility (Pai, 1965a; Pai, 1965b). As can be seen in Fig. 1D, although the bones of paralyzed *Vegf*-OE mice exhibited aberrant mineral deposition, they did not break. This result strongly supports the hypothesis that developing bones are exposed to significant intrauterine muscle forces.

Intriguingly, the patterns of the fractures in each of the bones of the *Vegf*-OE mice were consistent both in location and in fragment orientation. This provides an indication for the probable direction of the bending load acting on the bone. For example, the femora always fractured at the center of their diaphysis, such that they bent in the lateral-medial plane with their lateral aspect in tension and medial aspect in compression. The same bowing direction of the femur was also noted in another mutant mouse strain in which the ossification process is altered, namely the *Runx2* heterozygote (data not shown; to be

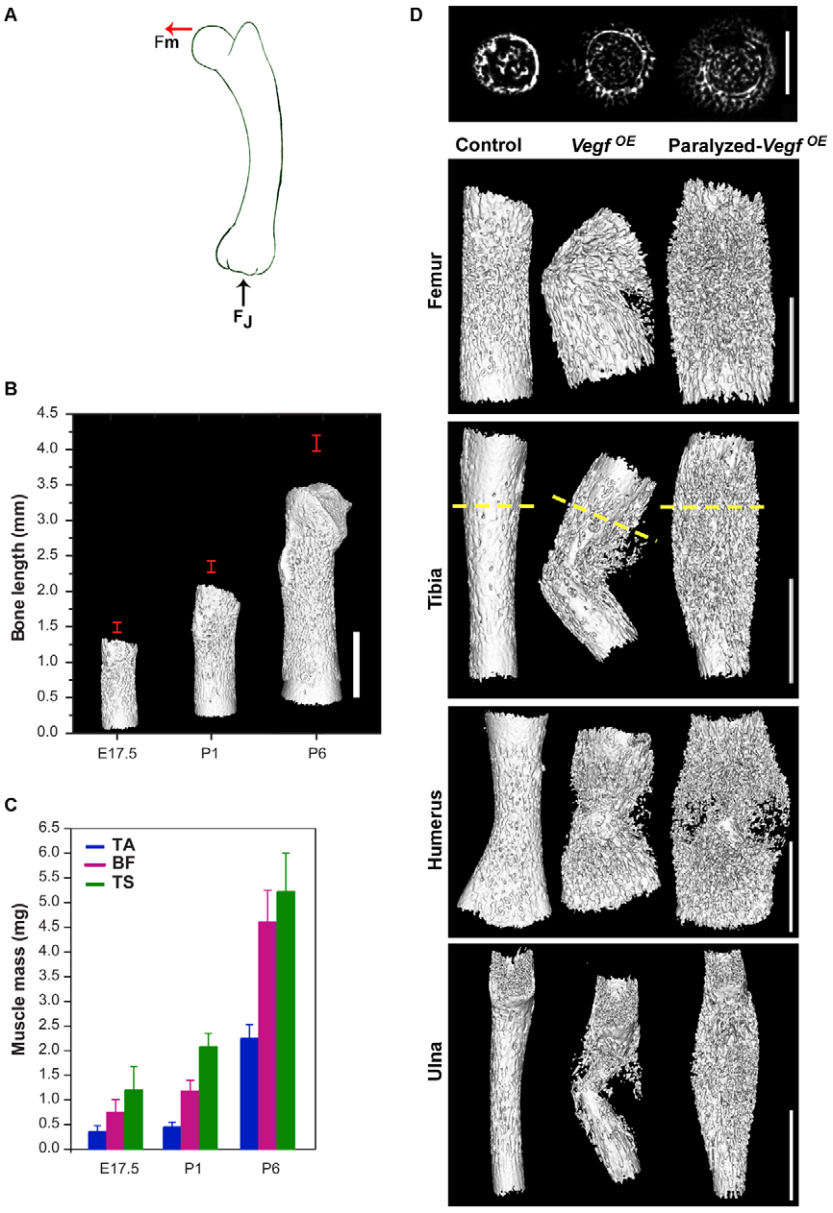

Fig. 1. Forming bones are exposed to increasing stresses caused by rapidly increasing muscle forces. (**A**) Illustration of the bending loads acting on the bone. F_m, muscle force; F_J, joint reaction force. (**B**) The increase in mouse femora length between E17.5 and P6. (**C**) The mean increase in mass of three representative muscles between E17.5 and P6. TA, tibialis anterior; BF, biceps femoris; TS, triceps brachii. Error bars represent s.d. from the mean. (**D**) Three-dimensional reconstructions from micro-CT scans of various bones at E18.5 from control (left), *Vegf*-OE (middle) and paralyzed *Vegf*-OE (right) mice, with the Vegf-OE bone exhibiting spontaneous fractures. Cross-sectional view (top) of the tibial proximal regions (plane indicated by yellow dashed line) illustrates the abnormal arrangement of the primordial cortex in both mutants. Scale bars: 1 mm except in cross-sectional views in D (top): 500 μm.

reported elsewhere). This consistency suggests that although the loading regime of bones is the result of forces applied by a large number of muscles, which act in different directions and with different force magnitudes, the overall loading scenario affecting the femur is mediolateral bending.

Taken together, these results suggest that, in utero, the forming bones are exposed to increasing stresses caused by their own lengthening combined with rapidly increasing muscle forces and that aberrant mineralization results in bone fracture.

The spatial and temporal structural changes that occur during periosteal bone formation are highly conserved

The structure and mineral composition of mature bones enable them to withstand loads (Weiner and Wagner, 1998). However, the contribution of these factors to the load-bearing capacity of embryonic bones is unknown (Seeman, 2003). To assess this contribution, a detailed description of the course of structural and mineral changes during development is required. We performed daily micro-CT scans of appendicular long bones of mice during the prenatal to early postnatal period of E16.5 to P6 and analyzed these images as a sequence of snapshots of a continuous process.

Bones grow in width by the process of periosteal bone formation. This process commences at mid-diaphysis, from which the growth plate has already retreated. As can be seen in Fig. 2A, periosteal bone growth starts with the formation of a relatively cylindrical layer of mineral around the middle section of the cartilage core. Next, this bone collar expands centrifugally by a sequence of repetitive steps. First, periodically spaced mineralized struts are deposited, which are aligned perpendicularly to the exterior-most ring. Then, the next ring is constructed, supported upon these struts (Fig. 2B). This process forms a primordial cortex consisting of several strut-ring layers, which gradually becomes thicker and its outer perimeter increases (red lines in Fig. 2C,D).

Concomitantly with bone expansion, a complementary process of bone resorption commences. This process, which is exclusive to the inner, endosteal aspect of the cortex, leads to a gradual increase in inner perimeter and cortical porosity (black lines in Fig. 2C,D)

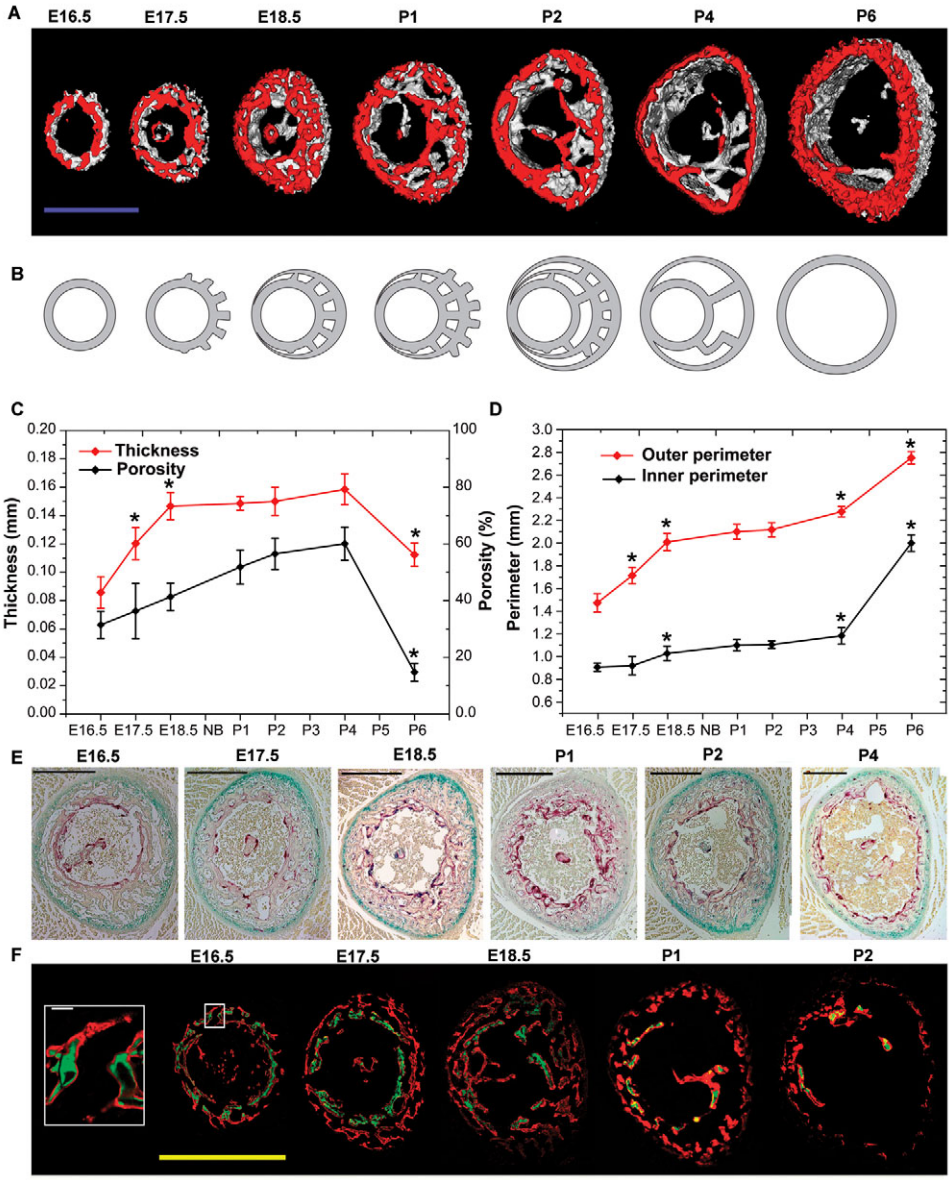

Fig. 2. The spatial and temporal structural changes that occur during periosteal growth are highly conserved. (**A**) Three-dimensional reconstructions of mouse mid-femoral diaphyses demonstrate the developmental phases of the primordial cortex (red). (**B**) Model of periosteal bone formation. Following the emergence of a rudimentary bone collar around the cartilage core, apposition occurs by repeated cycles of mineralized strut deposition and ring construction. Next, bone resorption commences at the endosteal aspect, which leads to a dramatic reduction in cortical thickness. (**C**,**D**) Changes in the thickness and porosity (C) and in the outer (periosteal) and inner (endosteal) perimeters (D) of the forming cortex from E16.5 to P6. Significant changes ($P \leq 0.05$) are marked with asterisks. Error bars indicate s.d. (**E**) Histological sections from the same region as in B stained to show the location of osteoblasts (green), which were present mostly along the periphery of the developing cortex, and of osteoclasts (purple), which were found to accumulate in the endosteum and inner cortical layers. (**F**) Histological sections from the same region as in B and E subsequent to the injection of Calcein (green) at E15 and Alizarin Complexone (red) at E16. Regions of bone deposition and resorption correspond to those detected by micro-CT. Inset shows the boxed area (E16.5) at higher magnification. Scale bars: 500 μm in A,F; 200 μm in E; 20 μm in F inset.

and eventually to a dramatic reduction in cortical thickness (Fig. 2A, right; Fig. 2C, red line). As a result, at P6 the primordial cortex is thinner than at E18.5.

With minor variations in time and magnitude, this characteristic sequence of periosteal growth and endosteal resorption was evident in all the bones examined (see Fig. S2A,B in the supplementary material). In order to more precisely determine the spatial distribution of bone formation and resorption, we analyzed by histological staining the distribution of osteoblasts and osteoclasts during early bone development. Histological sections revealed that osteoblasts were present mostly along the periphery of the developing cortex and only barely within the cortex itself (green stain in Fig. 2E). By contrast, osteoclasts accumulated in the endosteum and inner layers of the cortex (purple stain in Fig. 2E). Mineral deposition and resorption were also examined by injecting fluorochromes of different colors into pregnant females twice during gestation, at E15.5 and at E16.5. As shown in Fig. 2F, the results corresponded to the pattern suggested by micro-CT analysis. Extensive bone deposition was evident between E16.5 and E18.5, followed by a rapid resorption at the inner cortex.

Bone shape is regulated by preferential periosteal growth

Intriguingly, our analysis revealed that the cross-sections of all examined bones were clearly not circular, exhibiting a variety of circumferential outlines (Fig. 3A). This suggests that periosteal bone formation is a preferential process, in the sense that not all the sectors of the bone shaft grow in width at the same rate, resulting in a non-uniform circumference.

To validate this hypothesis, local patterns and rates of periosteal bone growth around the circumference of the forming cortex were quantitatively analyzed using a polar coordinate system superimposed on diaphyseal cross-sections (see Materials and methods). In all the different long bones we evaluated, the rate of periosteal bone growth was not uniform circumferentially. Growth rate in certain sectors was up to 5-fold higher than in others, resulting in a thicker cortex in these regions. Consequently, these regions also exhibited an increase in the distance between the geometric center of the bone at the earliest evaluated stage (E16.5) and the outer perimeter, which is referred to as the appositional radius (Fig. 3B,C and see Fig. S3A in the supplementary material).

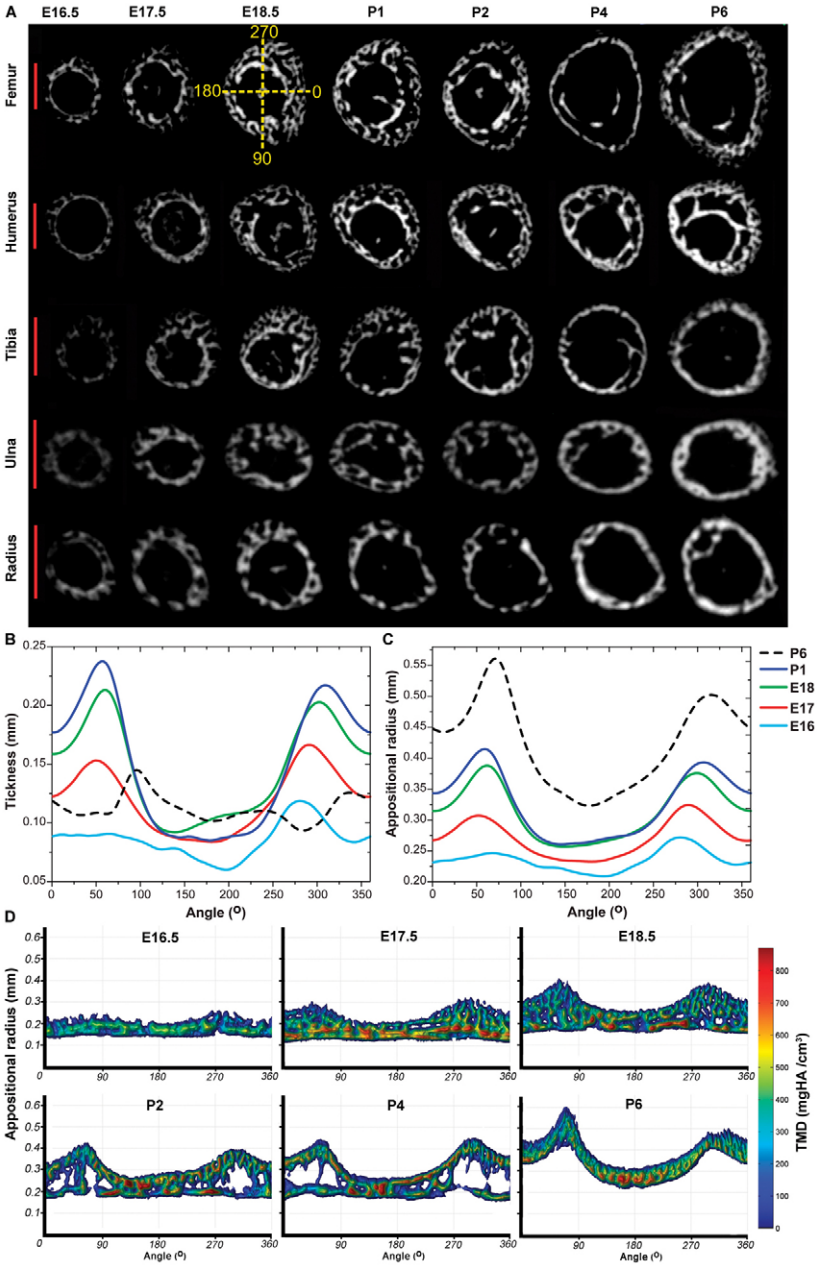

Fig. 3. Bone shape is regulated by preferential periosteal growth and mineral accretion. (**A**) Representative cross-sectional micro-CT images from an identical diaphyseal location in several mouse long bones from E16.5 to P6. Images of each bone type are plotted on the same intensity scale for direct comparison. As demonstrated by the yellow axes superimposed on the E18.5 femur, a polar coordinate system was used to assess growth parameters along the circumference of the cortex (see Materials and methods for definitions). In every bone, the preferential nature of periosteal growth caused a transition from an early cylindrical cross-section to an oval-like cross-section, thereby serving as a shaping mechanism. Scale bars: 500 μm. (**B**,**C**) The cortical thickness and appositional radius of the femoral cross-sections in Fig. 2A as a function of angular coordinate (degrees), representing the location on the circumference of the primordial cortex. The growth rate in certain sectors was up to 4-fold higher than in others, resulting in a thicker cortex and, consequently, an increased appositional radius in these regions; in other sectors, growth was barely detectable. (**D**) Analysis of micro-CT scans shows mineral distribution through the developing cortex as a function of angular coordinate. Previously thinner regions of the primordial cortex exhibited higher levels of mineral compared with formerly thicker regions. Color scale indicates the relative concentration of mineral (red, high; blue, low).

Interestingly, in some sectors, growth was barely detectable. For example, the cranial region (180°) of the femoral primordial cortex increased in thickness from 0.07 mm to 0.10 mm between E16.5 and P1, whereas during the same period the lateral region (60°) grew from 0.08 mm to 0.24 mm (Fig. 3A-C). A comparison of all the long bones evaluated indicated that it was the concave aspect of the bone or close to areas of bone protrusions that exhibited the increased growth rate (see Fig. S4 in the supplementary material).

Our finding that periosteal growth is an asymmetric, preferential process prompted us to search for distinctive variations in mineral density distribution within developing bones, which have not been described so far. We used a novel technique that we term ‘unroll transformation’, which enables analysis of the 3D spatial distribution of mineral density levels in bones (see Fig. S5 in the supplementary material). We found that the pattern of mineral density distribution was highly conserved. As can be seen in Fig. 3D, sectors in which growth was minimal exhibited higher mineral density, whereas sectors of rapid growth exhibited lower mineral density. Examination of other long bones revealed conserved patterns of mineral distribution that were unique to each bone type (as demonstrated by the tibia in Fig. S3B in the supplementary material).

Together, our results clearly suggest that the preferential nature of periosteal bone growth causes a transition from an early cylindrical cross-section to an oval-like cross-section, thereby serving as a mechanism that shapes bones.

Preferential periosteal growth enables bones to withstand increasing bending load

Having established that preferential periosteal growth shapes the circumferential outline of the forming bones, we proceeded to assess the contribution of this process to the bending strength of the bone. We compared, using finite element analysis (see Materials and methods), the strains that occur in three models representing variations in bone morphology: model A had the geometry of an

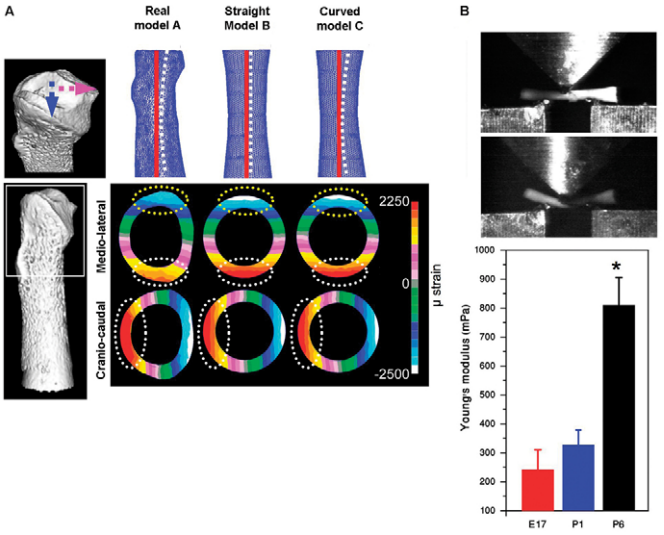

Fig. 4. Preferential periosteal growth enables bones to withstand increasing bending loads. (**A**) Schematic (top) showing the structure of the three models evaluated by finite element analysis: real model A, an actual mouse P6 femur; straight model B, a straight symmetrical tube; and curved model C, a curved symmetrical tube. White dotted lines demonstrate the curvature of the model with respect to the red vertical lines. To the left is shown a 3D reconstruction of P6 femur (a higher magnification of the boxed area illustrated beneath), demonstrating the loading directions of the models: pink arrow, mediolateral bending; blue arrow, craniocaudal bending. Strain maps (bottom) are shown in cross-sections taken from the mid-diaphysis of the three models, which were loaded physiologically (mediolateral, top row) and in the orthogonal direction (craniocaudal, bottom row). The color scale indicates the range of strain magnitudes; tensile strains are represented by positive values and compressive strains by negative values. When loaded by a physiological bending force, lower compressive strains (yellow dotted circles) and lower tensile strains (white dotted circles) were detected in the actual model as compared with the curved and straight tube models. (**B**) Images (top) of a three-point bending test performed on an E17 bone. The moving anvil is shown making contact with the bone; the lower image was taken immediately after fracture. Young's modulus (bottom) calculated by three-point bending test. Error bars represent s.d. from the mean; significant differences ($P \leq 0.05$) between consecutive points are marked with an asterisk.

actual wild-type (WT) P6 femur; model B was a straight tube with a circular cross-section; and model C was a tube similar to model B but curved similarly to the actual femur. To isolate the influence of preferential bone growth and eliminate the effect of mineral distribution, all the models had the same length, cross-sectional cortical area and material stiffness. Based on fragment orientation in the fractured *Vegf*-OE bones described above, two loading scenarios were tested: a physiological, mediolateral bending force and a non-physiological, craniocaudal bending force (Fig. 4A).

The results showed that under physiological bending force, the axial strains in the model of the actual bone were lower than in both idealized tubes, especially in the mid-diaphysis region (Fig. 4A). Also, the axial strains in the curved tube were less than those in the straight tube. However, both trends were reversed when the loading direction was orthogonal to the physiological loading direction. These results suggest that under physiological loads, preferential periosteal growth forms a 3D structure that makes the bone better adapted mechanically.

In addition to assessing the effect of morphology on bending strength, we determined the mechanical properties of the developing bone material by performing three-point bending tests on radii from mice at various ages. As can be seen in Fig. 4B, our analysis revealed that during development bone material becomes progressively stiffer, by a factor of 4: from an average Young's modulus of 242 MPa at E17.5 to 810 MPa at P6. This increase is probably due to increased mineral density as well as to a decreased occurrence of micro-voids within the bone. The values determined at E18.5 and P6 were incorporated into the finite element models.

Taken together, our results support the hypothesis that the structure and composition of the developing bone improve its ability to withstand rapidly increasing loads applied by muscle forces in utero.

Intrauterine muscle forces regulate preferential periosteal growth for optimal load-bearing capacity

An intriguing question raised by our finding that preferential periosteal growth is the developmental program that forms the typical circumferential outline of each bone is how this program is regulated. Since we hypothesize that the 3D shape of a bone improves its load-bearing capacity, an attractive possibility is that muscle forces regulate this program in utero. To test this hypothesis, we examined this process in the mdg mouse, which lacks skeletal muscle contractility (Pai, 1965a; Pai, 1965b). The mdg mice die perinatally; therefore, only bones from E17.5 embryos to newborn mice were analyzed.

It is a generally accepted principle that areas of accelerated bone formation coincide with sites at which peak strain magnitudes occur (Levenston et al., 1998; Nowlan et al., 2007). mdg embryos grow in a relatively load-free uterine environment, where strain levels must be low. We therefore expected to find an overall reduction in the rate of periosteal expansion in these mutants. However, overall cortical thickness in mdg bones was comparable to that in age-matched WT mice (Fig. 5A) or even greater, as in the case of the humerus (see Fig. S6A in the supplementary material) and radius (not shown). Next, we examined whether the characteristic preferential nature of periosteal growth occurred in bones of mdg mice. In the absence of contracting musculature, the developing bone shafts failed to gain an oval-like cross-section and maintained their almost circular cross-section, thereby losing the stereotypical circumferential outline of each bone type (Fig. 5B,B′,B″). To quantify these morphological differences, the ratio between the maximum and minimum cross-sectional moments of inertia (Imax/Imin), which reflects the deviation in shape from circularity (Carlson, 2005), was measured. This ratio was much higher in WT than mdg mice; for example, the ratio was 1.47 in the femur of WT mice as compared with 1.07 in newborn paralyzed mice (Fig. 5C,C′ and see Fig. S6B in the supplementary material).

Quantitative analysis of local patterns and rates of periosteal bone growth showed that this process was indeed much more uniform in mdg mice than in WT mice. Interestingly, this was not only due to a lack of localized accelerated thickening, but also to the absence of sectors where growth was quiescent (Fig. 5D and see Fig. S6C in the supplementary material). Examination of the differences in mineral density between WT and mdg bones revealed a 10-20% decrease in the mutant (Fig. 5E and see Fig. S6D in the supplementary material). Moreover, the uniformity of growth in mdg bones was also manifested in an even distribution of mineral density, unlike the pattern observed in control bones (Fig. 5F).

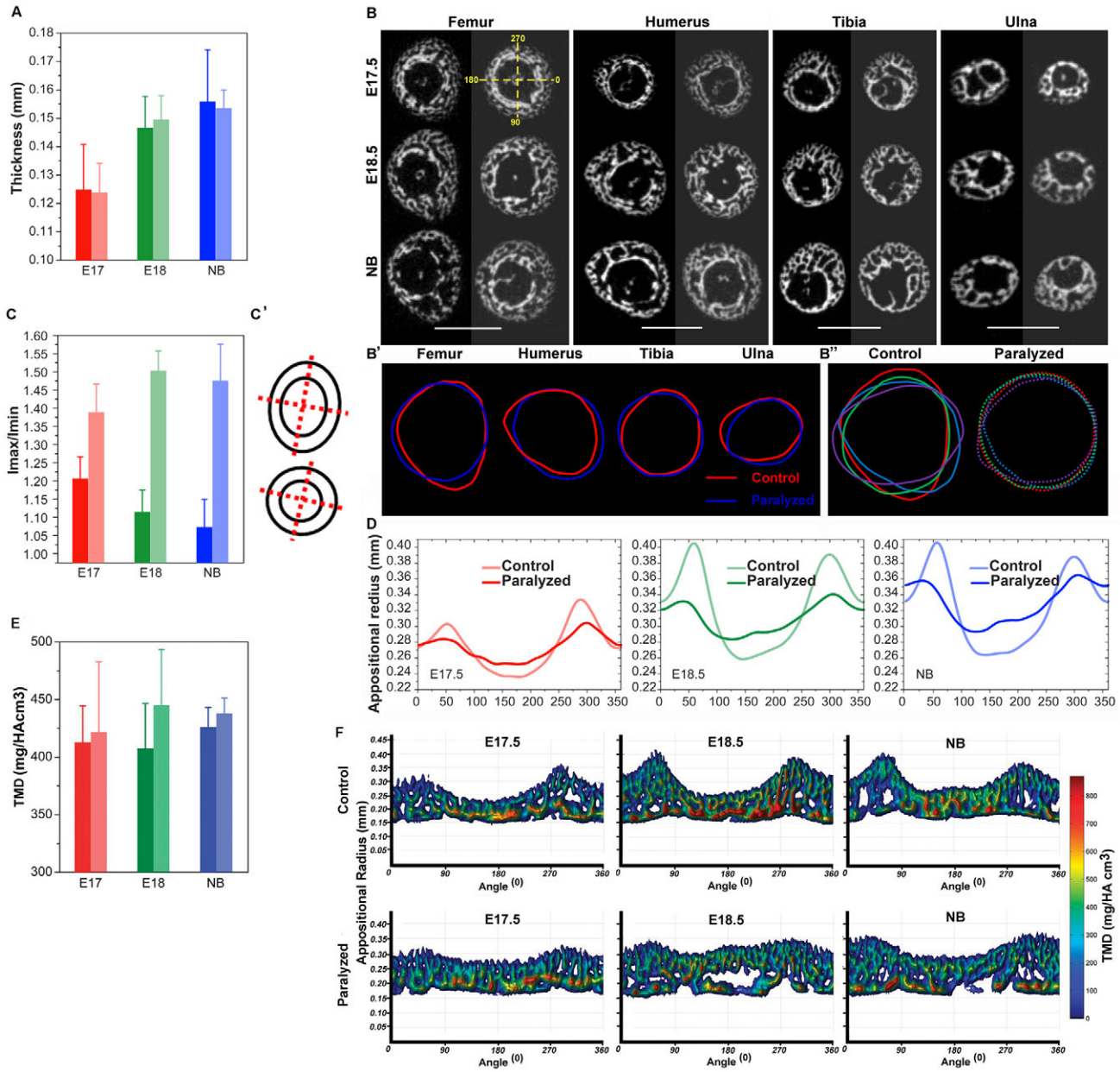

Fig. 5. A central role for muscle loads in regulating periosteal bone growth and morphogenesis in utero. (**A**) Comparison of the mid-diaphyseal cortical thickness of paralyzed (darker shade) and control (lighter shade) femora of E17.5, E18.5 and newborn (NB) mice. No significant differences were found in the overall thickness of the primordial cortex. (**B**) Micro-CT cross-sectional images from an identical diaphyseal location in bones from paralyzed (right) and control (left) mice. Scale bars: 500 μm. (**B′**) Superimpositions of the circumferential outlines of the cross-sections in B highlight the differences in appositional growth between control (red) and paralyzed (blue) newborn mice. (**B″**) Superimpositions of size-adjusted bone outlines from control (left) and paralyzed (right) mice. Each bone type is represented by a different color. Whereas each bone of the control has a unique pattern of growth, appositional growth in the paralyzed mouse was much more uniform. (**C**) The ratios of the maximum and minimum second moment of inertia of paralyzed (darker shade) and control (lighter shade) femora. (**C′**) Schematic demonstration of the measured maximum and minimum cross-sectional moment of inertia in the control (top) and paralyzed (bottom) mice. (**D**) The femoral appositional radius as a function of angular coordinate in paralyzed and control mice, as measured from the micro-CT cross-sections. (**E**) Bone mineral density in paralyzed (darker shade) and control (lighter shade) femora at E17.5, E18.5 and newborn. (**F**) Analysis of micro-CT scans showing mineral distribution in the developing cortex as a function of angular coordinate in paralyzed (bottom row) and control (upper row) femora. The color scale indicates mineral concentration (red, high; blue, low). Error bars indicate s.d.

Together, these results support a central role for muscle loads in regulating periosteal bone growth and morphology in utero.

As mentioned above, we hypothesize that intrauterine regulation of periosteal bone growth by muscle loads brings about a structure that is better adapted to withstand these loads. This implies that mdg bones, which develop in the absence of muscle contractions and lack the stereotypical circumferential outline, are expected to be mechanically inferior to WT bones in their ability to cope with physiological loads. To put this assumption to the test, we again used finite element analysis and compared strain distributions

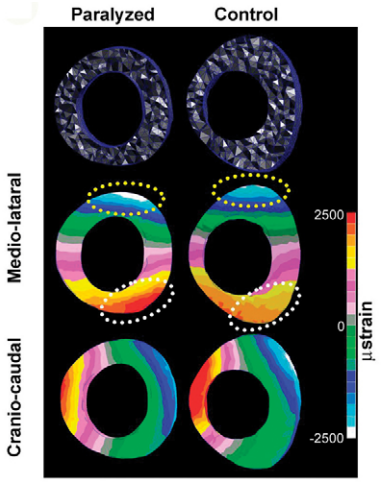

Fig. 6. Intrauterine muscle forces regulate preferential periosteal growth for optimal load-bearing capacity. Three-dimensional meshed finite element model (top row) and strain maps (beneath) of paralyzed (left) and control (right) femora at E18.5. Loading was physiological (mediolateral) or in the orthogonal direction (craniocaudal); the color scale shows strain distribution, with compressive strains represented by negative values and tensile strains by positive values. When loaded by a physiological bending force, lower compressive strains (yellow dotted circles) and lower tensile strains (white dotted circles) were detected in the control model as compared with the paralyzed model.

predicted to occur in E18.5 femora of WT and mdg mice. As can be seen in Fig. 6, under a mediolateral bending load, significant changes are predicted in the distribution and range of axial strains in the mid-diaphysis of E18.5 mdg femora. Higher compressive and tensile axial strains were detected in most regions of the mdg femoral mid-diaphysis, as compared with those of the WT. An opposite effect was observed when the models were loaded by a craniocaudally directed force.

These results support our hypothesis that mechanical loads applied in utero lead to the development of a structure that is better adapted to cope with these loads.

Preferential periosteal growth is mediated by a local increase in osteoblast number

The shape of a bone is modulated by the activity of osteoclasts and osteoblasts (Rauch, 2006). To study the effect of intrauterine muscle load on these cells, we first examined osteoclast number and distribution across the developing bones in the absence of muscle contraction. TRAP staining of bones from control and mdg mice showed similar osteoclast numbers and distribution (Fig. 7A). However, the cross-sectional marrow area, which is considered the result of osteoclast activity, was significantly lower in mdg mice (Fig. 7B). This suggests that, although osteoclast number was not affected by the absence of intrauterine muscle load, their activity was reduced.

To study the influence of osteoclasts on the circumferential shape of bones, we examined periosteal growth in *Src*-null mice, which lack osteoclast activity (Soriano et al., 1991). As can be seen in Fig. 7C, although *Src*-null mice exhibited abnormalities in bone modeling and growth, their bones did undergo preferential periosteal growth and had circumferential outlines similar to those of control bones.

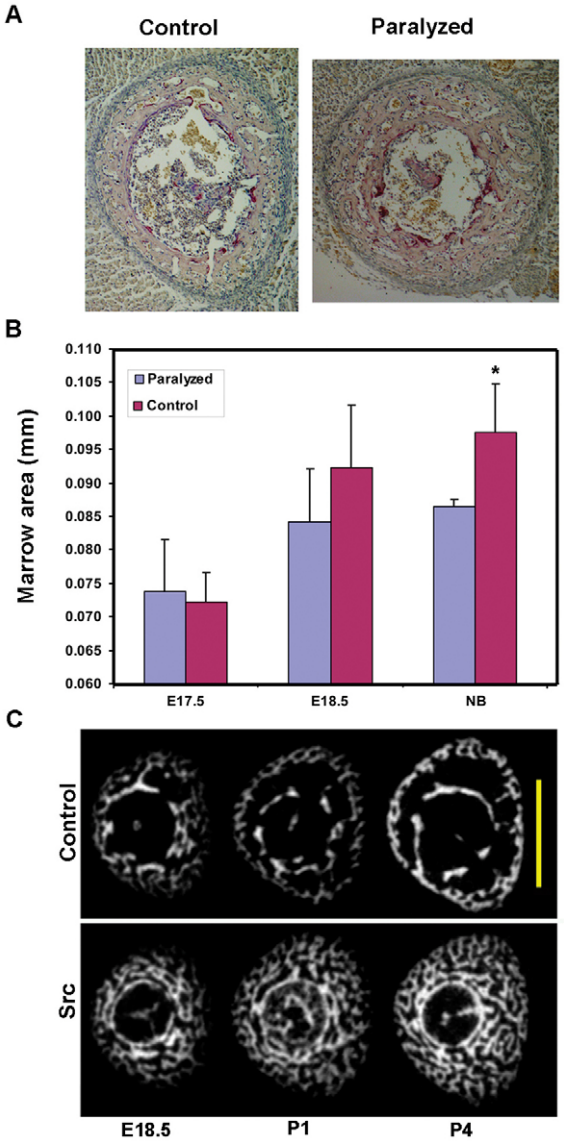

Fig. 7. Osteoclast activity is reduced in paralyzed mice. (**A**) Histological sections from the diaphyseal region of femora of paralyzed and control mice at E18.5, TRAP-stained for osteoclasts. No difference in osteoclast distribution was observed between paralyzed and control mice. (**B**) The changes in marrow area of the forming femur of paralyzed and control mice from E17.5 to birth. Error bars represent s.d. from the mean; significant changes between control and paralyzed mice are marked with asterisks ($P \leq 0.05$). Whereas at E17.5 there is no difference between paralyzed and control mice, by birth the marrow area is notably smaller in the mutant. (**C**) Micro-CT images from an identical mid-diaphyseal location in the femora of E18.5, P1 and P4 osteoclast-deficient (*Src*-null) mice and control (WT) littermates. Although resorption from the inner surface of the bone collar is missing in the *Src*-null mice, periosteal growth is almost unaffected, resulting in a normal outer outline. Scale bar: 500 μm.

Together, these results imply that osteoclast function is affected by muscle load. However, whereas resorption in the marrow cavity is affected in the absence of muscle contraction, osteoclast activity does not play a major role in regulating bone preferential growth and circumferential outline.

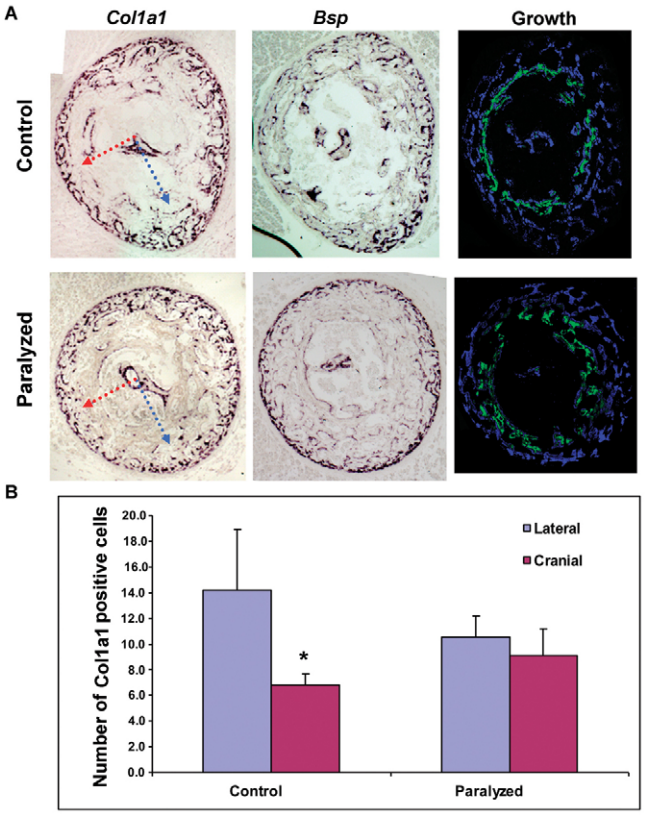

Fig. 8. Osteoblast distribution is controlled by mechanical load. (**A**) In situ hybridization for the osteoblastic markers *Col1a1* (left) and *Bsp* (right) at femoral mid-diaphysis (as in Fig. 5B). The numbers of *Col1a1*-positive cells in the lateral sector (blue arrow), which underwent extensive growth, and cranial sector (red arrow) of quiescent growth, were compared. To the right are shown histological sections from the same regions as in the left panels, subsequent to the injection of Calcein (green) at E15 and of Calcein Blue (blue) at E17. (**B**) Whereas in paralyzed mice there was no difference in *Col1a1* expression between these sectors, in control mice there were more than twice as many osteoblasts in the region that expanded quickly than in the quiescent growth sector (n=4). Error bars represent s.d. from the mean; significant changes (P≤0.05) are marked with asterisks.

Next, we examined the distribution of osteoblasts as a possible mediator of mechanical signals during bone shaping. We performed in situ hybridization for the osteoblastic markers *Col1a1* and *Bsp* (*Ibsp* – Mouse Genome Informatics). In control mice, we observed a greater than 2-fold increase in the *Col1a1*- and *Bsp*-positive cell count at sectors that underwent fast preferential bone growth (Fig. 8A, upper panels, blue arrow; Fig. 8B), as compared with sectors where growth was quiescent (red arrow). By contrast, no difference in the distribution of osteoblastic markers was noted in mdg mice (Fig. 8A, bottom panels; Fig. 8B). Injection of fluorochromes of different colors into pregnant mice (Fig. 8A, right panel) demonstrated these differences in growth.

These results suggest that muscle contraction is required to induce differential osteoblast distribution around the cortex, which results in differential growth rates in different sectors.

DISCUSSION

A basic question in organ morphogenesis is how the genetic program interacts with environmental signals such as mechanical forces. The involvement of mechanical load in bone development has been the subject of a long-standing debate (Guenther et al., 2008; Hall, 1971; Murray and Selby, 1930; Nowlan et al., 2008; Klein-Nulend et al., 1986). To unravel the contribution of mechanical forces to bone morphogenesis, it is first necessary to determine the magnitude of the forces acting on developing bones, their source and the onset of this effect. Second, a detailed description of the morphogenetic sequence that bones undergo during development is required. Such a description is a prerequisite for an assessment of the effects of mechanical forces on the morphogenetic process through experimental manipulations. Finally, the cellular and molecular mechanisms that integrate the mechanical signals with the genetic program that regulates the morphogenetic process have to be identified.

Embryonic movement is a reliable indicator for the onset of muscle contraction. Chick embryos start to move as early as 4-5 days incubation, whereas in murine embryos movement is observed by E12.5 (Bennett et al., 1983; Carry et al., 1983; Hamburger and Balaban, 1963; Suzue, 1996). Although it is clear that the skeleton experiences mechanical loads exerted by muscle contraction through most of its development, the magnitude of these loads has not been appreciated. The increase in lever arm as a result of bone elongation has been neglected too. We show that the combined result of increased muscle mass and longer lever arm is a ~15-fold increase in the potential bending moment applied by muscles on bones. Moreover, we provide evidence that muscle contraction exerts substantial mechanical loads on the skeleton, such that abnormal bone development can lead to structural failure. Intrauterine fractures of long bones have also been reported in several other strains of mice in which the ossification process is altered (Pereira et al., 1994). Given our initial estimation of the mechanical loads acting on the developing skeleton, we postulated that bones accommodate these loads by adapting their morphology. Indeed, finite element analysis clearly supports the hypothesis that the morphology of developing bones allows them to cope better with the increasing loads.

The involvement of embryonic movement and muscle contraction in skeletogenesis was reported as early as 1901 (Herbest, 1901). The contribution of these factors to the formation of joints and bone eminences has been well established (Drachman and Sokoloff, 1966; Fell and Canti, 1943; Hamburger and Waugh, 1940; Mikic et al., 2000; Murray and Drachman, 1969; Hasty et al., 1993; Osborne et al., 2002; Pai, 1965a; Tremblay et al., 1998). However, the contribution of muscle contraction to bone morphogenesis has attracted little attention.

One of the main obstacles in evaluating the contribution of muscle contraction to bone morphology is the lack of an accurate description of the morphogenetic process itself. That is, the morphological sequence that the developing bone undergoes, from the onset of the ossification process to the emergence of a mature, fully ossified bone, has been missing. The increased use of micro-CT as an imaging modality that provides a representation of the entire 3D structure of a bone has provided the opportunity to document bone morphology at different stages of development. Using micro-CT images of developing bones and new image analysis algorithms (to be reported elsewhere), we present a more comprehensive model of bone formation, which incorporates the contribution of preferential periosteal growth to bone morphology (Fig. 9).

Equipped with a better understanding of the magnitude of intrauterine muscle forces acting on developing bone and a more inclusive model of bone development, we revisited the question of the effect of the contracting musculature on the morphology of long bones. We demonstrate the importance of muscle contractions in

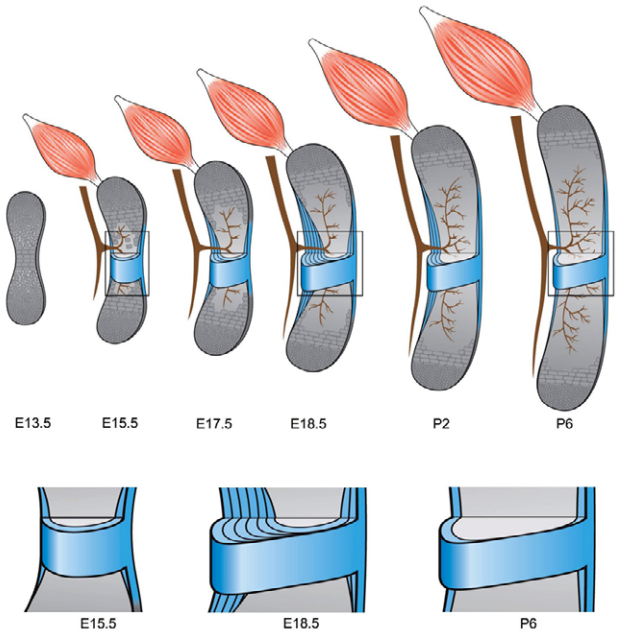

Fig. 9. Model of mouse embryonic bone development. At E13.5, differentiation of mesenchymal cells into chondrocytes forms an avascular cartilage template of the future bone. At E14.5, chondrocytes in the center of the cartilage template mature to hypertrophy. Meanwhile, skeletal muscles connect to the cartilage and exert force upon it. One day later, sprouting blood vessels, osteoclastic cells and hematopoietic precursors begin to invade the hypertrophic cartilage. In the perichondrium, a relatively cylindrical sleeve of mineral (the bone collar) forms around the cartilage core. At later stages, the marrow cavity expands by continued erosion of the hypertrophic cartilage in the growth plates at both ends of the growing bone. As the hypertrophic cartilage is removed, it is replaced by trabecular bone in the regions beneath the growth plate. This process results in bone lengthening. At the same time (E15.5-18.5), the bone collar expands centrifugally by periosteal bone formation, as a primordial cortex, consisting of several strut-ring layers, is being formed. The preferential nature of this apposition process leads to the typical shape of the bone shaft. Finally, resorption of the endosteal surface results in a thinner cortex (P6), which has already adopted the typical shape of the bone. The mid-diaphyseal regions at E15.5, E18.5 and P6 (boxed) are magnified beneath to illustrate the transient nature of cortical thickening.

regulating differential mineral deposition in the forming bone, which results in the formation of a stereotypical circumferential outline for each bone. The significance of this regulation is not restricted to the morphological aspect, as evidenced by the contribution of the circumferential outlines of developing bones to their mechanical competence.

Surprisingly, muscle contraction not only promoted accelerated bone growth, as would be expected (Levenston et al., 1998; Nowlan et al., 2007), but also inhibited it. This finding suggests the existence of a mechanism that translates strain into different, context-dependent signals, leading to different biological outputs. Little is known in vivo about the molecular mechanisms that translate mechanical signals into biological outputs. One obvious starting point for deciphering these mechanisms is to explore the role of the cells involved in bone morphogenesis, namely osteoblasts and osteoclasts.

Our cellular analysis reveals that periosteal growth is spatially correlated with increased numbers of osteoblasts, under regulation of mechanical load. Since we failed to observe osteoclasts in the periosteum or changes in the circumferential outline of *Src* mutant bones, we conclude that osteoblasts are the main cellular component in the mechanism that responds to the load exerted by muscle contraction. Interestingly, however, the decrease we found in marrow area in paralyzed mice suggests that osteoclast function is also influenced by mechanical load. This finding might be explained by a possible link between this mechanism and the Wnt/β-catenin signaling pathway. Mechanical load has been shown to increase the activity of this pathway (Robinson et al., 2006). Moreover, activation of this pathway has been shown to promote osteoblast differentiation and inhibit osteoclast differentiation (Glass et al., 2005). These observations make the Wnt/β-catenin pathway a promising candidate for signaling between muscle contraction and localized periosteal growth.

Based on these findings, we suggest that the coupling between muscle contraction and bone morphogenesis via a mechanism that translates mechanical signals into the differential distribution of bone-forming cells is fundamental in regulating bone morphology. This coupling might serve to accelerate evolutionary changes in bone morphology.

Interestingly, we identify several surprising deviations from the common view of bone development. The first is the notion that during the course of development, cortex thickness is either increased or maintained. We demonstrate that between E16.5 and E18.5 cortex thickness increases, but then sharply decreases almost to its initial thickness. We suggest that the temporary thickening of the cortex might serve to rapidly increase the outer diameter of the forming bone so as to improve its mechanical performance (Seeman and Delmas, 2006). The subsequent thinning might serve several functions, such as a reduction of bone mass to decrease metabolic costs or to facilitate increasing the marrow space. Reduction in cortical thickness is also described in infants during the first months of life (Rauch and Schoenau, 2001).

The second paradigm challenged by our findings regards the process of bone modeling during development. Bone modeling involves growth and resorption, which occur simultaneously on separate surfaces, and has been previously suggested as a mechanism for bone shaping (Enlow, 1962; Guenther et al., 2008). For example, accelerated radial bone growth on the convex side of the ribs and resorption on the concave side has been suggested to form their curvature (Epker and Frost, 1966). However, in our study, osteoclasts were observed only in the endosteum and not at the peripheral surface, suggesting that bone resorption at the concave periosteal surface does not participate in bone shaping at the early stages of development. Moreover, unlike in the rib, accelerated bone growth was detected on the concave rather than convex side of all long bones. This difference clearly suggests that preferential periosteal growth cannot be the mechanism by which the curvature of long bones is achieved.

This study identifies preferential periosteal growth as a mechanism by which long bones acquire their 3D morphology and mechanical properties during early stages of skeletogenesis and suggests a new model for the formation of long bones (Fig. 9). We show that the 3D morphology of a forming bone is affected by the reciprocal relationship that exists in utero between structure and mechanical load, as the structure of the bone determines the loads that it can tolerate, and loads determine the structure. Finally, we establish a new set of parameters that characterize the process of periosteal bone formation. These features might serve as the

foundation for further analysis of preferential circumferential growth, most importantly to identify the components of the mechanism that senses and translates the effect of mechanical load into signals that determine 3D bone morphology.

Acknowledgements
We thank G. Kern for the mdg mice; M. Barak, J. C. Currey, B. Olsen and C. J. Tabin for their helpful reviews of the manuscript; N. Konstantin for expert editorial assistance; S. Kerief for expert technical support; all members of the E.Z. laboratory for advice and suggestions; G. Brodsky from the Graphic Design Department of Weizmann Institute of Science for help with the graphic model; B. Pasmantirer from the Instrument Design Department of Weizmann Institute of Science for designing the mechanical testing apparatus; and D. Mintz from the Koret School of Veterinary Medicine for expert confocal microscopy imaging. This work was supported by grants from the Israel Science Foundation (ISF, grants 1206/09 to E.Z. and 151/8 to R.S.), Minerva Foundation (grant M1138), The Y. Leon Benoziyo Institute for Molecular Medicine, Helen and Martin Kimmel Institute for Stem Cell Research, J & R Center for Scientific Research, Kirk Center for Childhood Cancer and Immunological Disorders, Yeda-Sela Center for Basic Research, Estate of Raymond Lapon, Estate of David Levinson, ISF-Legacy Heritage Fund Morasha Bio-Medical program, The Leo and Julia Forchheimer Center for Molecular Genetics, and Marla L. Schaefer, New York, NY, USA.

Competing interests statement
The authors declare no competing financial interests.

Supplementary material
Supplementary material for this article is available at
http://dev.biologists.org/lookup/suppl/doi:10.1242/dev.063768/-/DC1

References
Belteki, G., Haigh, J., Kabacs, N., Haigh, K., Sison, K., Costantini, F., Whitsett, J., Quaggin, S. E. and Nagy, A. (2005). Conditional and inducible transgene expression in mice through the combinatorial use of Cre-mediated recombination and tetracycline induction. *Nucleic Acids Res.* **33**, e51.
Bennett, M. R., Davey, D. F. and Marshall, J. J. (1983). The growth of nerves in relation to the formation of premuscle cell masses in the developing chick forelimb. *J. Comp. Neurol.* **215**, 217-227.
Blitz, E., Viukov, S., Sharir, A., Shwartz, Y., Galloway, J. L., Pryce, B. A., Johnson, R. L., Tabin, C. J., Schweitzer, R. and Zelzer, E. (2009). Bone ridge patterning during musculoskeletal assembly is mediated through SCX regulation of Bmp4 at the tendon-skeleton junction. *Dev. Cell* **17**, 861-873.
Bradley, S. J. (1970). An analysis of self-differentiation of chick limb buds in chorio-allantoic grafts. *J. Anat.* **107**, 479-490.
Brear, K., Currey, J. D. and Pond, C. M. (1990). Ontogenetic changes in the mechanical properties of the femur of the polar bear Ursus maritimus. *J. Zool.* **222**, 49-58.
Carlson, K. J. (2005). Investigating the form-function interface in African apes: relationships between principal moments of area and positional behaviors in femoral and humeral diaphyses. *Am. J. Phys. Anthropol.* **127**, 312-334.
Carry, M. R., Morita, M. and Nornes, H. O. (1983). Morphogenesis of motor endplates along the proximodistal axis of the mouse hindlimb. *Anat. Rec.* **207**, 473-485.
Currey, J. D. (1999). The design of mineralised hard tissues for their mechanical functions. *J. Exp. Biol.* **202**, 3285-3294.
Currey, J. D. (2003). The many adaptations of bone. *J. Biomech.* **36**, 1487-1495.
Dacquin, R., Starbuck, M., Schinke, T. and Karsenty, G. (2002). Mouse alpha1(I)-collagen promoter is the best known promoter to drive efficient Cre recombinase expression in osteoblast. *Dev. Dyn.* **224**, 245-251.
Dor, Y., Djonov, V., Abramovitch, R., Itin, A., Fishman, G. I., Carmeliet, P., Goelman, G. and Keshet, E. (2002). Conditional switching of VEGF provides new insights into adult neovascularization and pro-angiogenic therapy. *EMBO J.* **21**, 1939-1947.
Drachman, D. and Sokoloff, L. (1966). The role of movement in embryonic joint development. *Dev. Biol.* **14**, 401-420.
Engleka, K. A., Gitler, A. D., Zhang, M., Zhou, D. D., High, F. A. and Epstein, J. A. (2005). Insertion of Cre into the Pax3 locus creates a new allele of Splotch and identifies unexpected Pax3 derivatives. *Dev. Biol.* **280**, 396-406.
Enlow, D. H. (1962). A study of the post-natal growth and remodeling of bone. *Am. J. Anat.* **110**, 79-101.
Epker, B. N. and Frost, H. M. (1966). Biomechanical control of bone growth and development: a histologic and tetracycline study. *J. Dent. Res.* **45**, 364-371.
Fell, H. and Canti, R. (1943). Experiments on the development in vitro of the avian knee joint. *Proc. R. Soc. Lond. B* **1176**, 316-351.
Frost, H. M. (2001). From Wolff's law to the Utah paradigm: insights about bone physiology and its clinical applications. *Anat. Rec.* **262**, 398-419.
Glass, D. A., 2nd, Bialek, P., Ahn, J. D., Starbuck, M., Patel, M. S., Clevers, H., Taketo, M. M., Long, F., McMahon, A. P., Lang, R. A. et al. (2005). Canonical Wnt signaling in differentiated osteoblasts controls osteoclast differentiation. *Dev. Cell* **8**, 751-764.
Gokhin, D. S., Ward, S. R., Bremner, S. N. and Lieber, R. L. (2008). Quantitative analysis of neonatal skeletal muscle functional improvement in the mouse. *J. Exp. Biol.* **211**, 837-843.
Guenther, C., Pantalena-Filho, L. and Kingsley, D. M. (2008). Shaping skeletal growth by modular regulatory elements in the Bmp5 gene. *PLoS Genet.* **4**, e1000308.
Hall, B. K. (1971). Histogenesis and morphogenesis of bone. *Clin. Orthop. Relat. Res.* **74**, 249-268.
Hall, B. K. and Kalliecharan, R. (1975). The effects of exogenous cortisone acetate on development (especially skeletal development) and on circulating levels of corticosteroids in chick embryos. *Teratology* **12**, 111-119.
Hamburger, V. and Waugh, M. (1940). The primary development of the skeleton in nerveless and poorly innervated limb transplants of chick embryos. *Physiol. Zool.* **13**, 367-384.
Hamburger, V. and Balaban, M. (1963). Observations and experiments on spontaneous rhythmical behavior in the chick embryo. *Dev. Biol.* **7**, 533-545.
Hasty, P., Bradley, A., Morris, J. H., Edmondson, D. G., Venuti, J. M., Olson, E. N. and Klein, W. H. (1993). Muscle deficiency and neonatal death in mice with a targeted mutation in the myogenin gene. *Nature* **364**, 501-506.
Herbest, C. (1901). Formative Reize in der tierischen Ontogenese. Leipzig: Georgi.
Hosseini, A. and Hogg, D. A. (1991). The effects of paralysis on skeletal development in the chick embryo. I. General effects. *J. Anat.* **177**, 159-168.
Kahn, J., Shwartz, Y., Blitz, E., Krief, S., Sharir, A., Breitel, D. A., Rattenbach, R., Relaix, F., Maire, P., Rountree, R. B. et al. (2009). Muscle contraction is necessary to maintain joint progenitor cell fate. *Dev. Cell* **16**, 734-743.
Karsenty, G. and Wagner, E. F. (2002). Reaching a genetic and molecular understanding of skeletal development. *Dev. Cell* **2**, 389-406.
Klein-Nulend, J., Veldhuijzen, J. P. and Burger, E. H. (1986). Increased calcification of growth plate cartilage as a result of compressive force in vitro. *Arthritis Rheum.* **29**, 1002-1009.
Komori, T., Yagi, H., Nomura, S., Yamaguchi, A., Sasaki, K., Deguchi, K., Shimizu, Y., Bronson, R. T., Gao, Y. H., Inada, M. et al. (1997). Targeted disruption of Cbfa1 results in a complete lack of bone formation owing to maturational arrest of osteoblasts. *Cell* **89**, 755-764.
Kronenberg, H. M. (2003). Developmental regulation of the growth plate. *Nature* **423**, 332-336.
Levenston, M. E., Beaupre, G. S. and Carter, D. R. (1998). Loading mode interactions in simulations of long bone cross-sectional adaptation. *Comput. Methods Biomech. Biomed. Eng.* **1**, 303-319.
Maes, C., Goossens, S., Bartunkova, S., Drogat, B., Coenegrachts, L., Stockmans, I., Moermans, K., Nyabi, O., Haigh, K., Naessens, M. et al. (2010). Increased skeletal VEGF enhances beta-catenin activity and results in excessively ossified bones. *EMBO J.* **29**, 424-441.
McClive, P. J. and Sinclair, A. H. (2001). Rapid DNA extraction and PCR-sexing of mouse embryos. *Mol. Reprod. Dev.* **60**, 225-226.
McLeod, M. J. (1980). Differential staining of cartilage and bone in whole mouse fetuses by alcian blue and alizarin red S. *Teratology* **22**, 299-301.
Mikic, B., Johnson, T. L., Chhabra, A. B., Schalet, B. J., Wong, M. and Hunziker, E. B. (2000). Differential effects of embryonic immobilization on the development of fibrocartilaginous skeletal elements. *J. Rehabil. Res. Dev.* **37**, 127-133.
Murray, P. D. and Selby, D. (1930). Intrinsic and extrinsic factors in the primary development of the skeleton. *Dev. Genes Evol.* **122**, 629-662.
Murray, P. D. and Drachman, D. B. (1969). The role of movement in the development of joints and related structures: the head and neck in the chick embryo. *J. Embryol. Exp. Morphol.* **22**, 349-371.
Murtaugh, J. (1999). Early detection. *J. Am. Dent. Assoc.* **130**, 624, 627.
Nowlan, N. C., Murphy, P. and Prendergast, P. J. (2007). Mechanobiology of embryonic limb development. *Ann. N. Y. Acad. Sci.* **1101**, 389-411.
Nowlan, N. C., Murphy, P. and Prendergast, P. J. (2008). A dynamic pattern of mechanical stimulation promotes ossification in avian embryonic long bones. *J. Biomech.* **41**, 249-258.
Olsen, B. R., Reginato, A. M. and Wang, W. (2000). Bone development. *Annu. Rev. Cell Dev. Biol.* **16**, 191-220.
Osborne, A. C., Lamb, K. J., Lewthwaite, J. C., Dowthwaite, G. P. and Pitsillides, A. A. (2002). Short-term rigid and flaccid paralyses diminish growth of embryonic chick limbs and abrogate joint cavity formation but differentially preserve pre-cavitated joints. *J. Musculoskelet. Neuronal Interact.* **2**, 448-456.
Pai, A. C. (1965a). Developmental genetics of a lethal mutation, Muscular Dysgenesis (Mdg), in the mouse. I. Genetic analysis and gross morphology. *Dev. Biol.* **11**, 82-92.
Pai, A. C. (1965b). Developmental genetics of a lethal mutation, Muscular Dysgenesis (Mdg), in the mouse. II. Developmental analysis. *Dev. Biol.* **11**, 93-109.
Pereira, R., Halford, K., Sokolov, B. P., Khillan, J. S. and Prockop, D. J. (1994). Phenotypic variability and incomplete penetrance of spontaneous fractures in an

inbred strain of transgenic mice expressing a mutated collagen gene (COL1A1). *J. Clin. Invest.* **93**, 1765-1769.
Rauch, F. (2006). Watching bone cells at work: what we can see from bone biopsies. *Pediatr. Nephrol.* **21**, 457-462.
Rauch, F. and Schoenau, E. (2001). Changes in bone density during childhood and adolescence: an approach based on bone's biological organization. *J. Bone Miner. Res.* **16**, 597-604.
Riddle, R. D., Johnson, R. L., Laufer, E. and Tabin, C. (1993). Sonic hedgehog mediates the polarizing activity of the ZPA. *Cell* **75**, 1401-1416.
Robinson, J. A., Chatterjee-Kishore, M., Yaworsky, P. J., Cullen, D. M., Zhao, W., Li, C., Kharode, Y., Sauter, L., Babij, P., Brown, E. L. et al. (2006). Wnt/beta-catenin signaling is a normal physiological response to mechanical loading in bone. *J. Biol. Chem.* **281**, 31720-31728.
Robling, A. G. and Turner, C. H. (2002). Mechanotransduction in bone: genetic effects on mechanosensitivity in mice. *Bone* **31**, 562-569.
Rubin, C. T. and Lanyon, L. E. (1984). Dynamic strain similarity in vertebrates; an alternative to allometric limb bone scaling. *J. Theor. Biol.* **107**, 321-327.
Schoenau, E. (2005). From mechanostat theory to development of the 'Functional Muscle-Bone-Unit'. *J. Musculoskelet. Neuronal Interact.* **5**, 232-238.
Schriefer, J. L., Robling, A. G., Warden, S. J., Fournier, A. J., Mason, J. J. and Turner, C. H. (2005). A comparison of mechanical properties derived from multiple skeletal sites in mice. *J. Biomech.* **38**, 467-475.
Seeman, E. (2003). Periosteal bone formation-a neglected determinant of bone strength. *N. Engl. J. Med.* **349**, 320-323.
Seeman, E. and Delmas, P. D. (2006). Bone quality-the material and structural basis of bone strength and fragility. *N. Engl. J. Med.* **354**, 2250-2261.
Shahar, R., Zaslansky, P., Barak, M., Friesem, A. A., Currey, J. D. and Weiner, S. (2007). Anisotropic Poisson's ratio and compression modulus of cortical bone determined by speckle interferometry. *J. Biomech.* **40**, 252-264.
Soriano, P., Montgomery, C., Geske, R. and Bradley, A. (1991). Targeted disruption of the c-src proto-oncogene leads to osteopetrosis in mice. *Cell* **64**, 693-702.
Srinivas, S., Watanabe, T., Lin, C. S., William, C. M., Tanabe, Y., Jessell, T. M. and Costantini, F. (2001). Cre reporter strains produced by targeted insertion of EYFP and ECFP into the ROSA26 locus. *BMC Dev. Biol.* **1**, 4.
Streeter, G. L. (1949). Developmental horizons in human embryos; a review of the histogenesis of cartilage and bone. *Contrib. Embryol.* **33**, 149-168.
Suzue, T. (1996). Movements of mouse fetuses in early stages of neural development studied in vitro. *Neurosci. Lett.* **218**, 131-134.
Tremblay, P., Dietrich, S., Mericskay, M., Schubert, F. R., Li, Z. and Paulin, D. (1998). A crucial role for Pax3 in the development of the hypaxial musculature and the long-range migration of muscle precursors. *Dev. Biol.* **203**, 49-61.
Turner, C. H. and Burr, D. B. (1993). Basic biomechanical measurements of bone: a tutorial. *Bone* **14**, 595-608.
Ward, K. A., Caulton, J. M., Adams, J. E. and Mughal, M. Z. (2006). Perspective: cerebral palsy as a model of bone development in the absence of postnatal mechanical factors. *J. Musculoskelet. Neuronal Interact.* **6**, 154-159.
Weiner, S. and Wagner, H. D. (1998). The material bone: structure-mechanical function relations. *Ann. Rev. Math. Sci.* **28**, 271-298.